Spatiotemporal Mapping of Early Volume Loss in the Mouse Brain after Cranial Irradiation

Authors: Ayoub, Ramy, Lau, Kaylie, Yuen, Nili, Fernandes, Darren, Elder, Madeline, et al.

Spatiotemporal Mapping of Early Volume Loss in the Mouse Brain after Cranial Irradiation

Ramy Ayoub,[a,d,e,1] Kaylie Lau,[d] Nili Yuen,[a,d,e] Darren Fernandes,[a,d,f] Madeline Elder,[d] Jonas Yeung,[a,d,e] Shun C. Wong[a,b,c,h] and Brian J. Nieman[a,d,e,g]

[a] Departments of Medical Biophysics and [b] Radiation Oncology and [c] Institute of Medical Science, University of Toronto, Ontario, Canada; [d] Mouse Imaging Centre, [e] Translational Medicine and [f] Neurosciences and Mental Health, The Hospital for Sick Children, Toronto, Ontario, Canada; [g] Ontario Institute for Cancer Research, Toronto, Ontario, Canada; and [h] The Sunnybrook Health Sciences Centre, Toronto, Ontario, Canada

Ayoub, R., Lau, K., Yuen, N., Fernandes, D., Elder, M., Yeung, J., Wong, S. C. and Nieman, B. J. Spatiotemporal Mapping of Early Volume Loss in the Mouse Brain after Cranial Irradiation. *Radiat. Res*. 196, 394–403 (2021).

Sequelae after pediatric cranial radiotherapy (CRT) result in long-term changes in brain structure. While past evidence indicates regional differences in brain volume change, it remains unclear how these manifest in the time course of change after CRT. In this study, we spatiotemporally characterized volume losses induced by cranial irradiation in a mouse model, with a dense sampling of measurements over the first week postirradiation. Wild-type mice received whole-brain irradiation (7 Gy) or sham irradiation (0 Gy) at 16 days of age. *In vivo* magnetic resonance imaging was performed at one time point before, and 2–4 time points postirradiation in each mouse, with a particular focus on sampling during the first week after cranial irradiation. Volume changes across the brain were measured, and the degree and timing of volume loss were quantified across structures from a predefined atlas. Volume measurements across the brain after cranial irradiation revealed a ~2-day delay in which volume is not significantly altered, after which time volume change proceeds over the course of four days. Volume losses were 3% larger and emerged 40% slower in white matter than in gray matter. Large volume loss was also observed in the ventricles. Differences in the timing and magnitude of volume change between gray and white matter after cranial irradiation were observed. These results suggest differences in the mechanism and/or kinetics underlying the associated radio-response, which may have implications in development. © 2021 by Radiation Research Society

[1] Address for correspondence: Mouse Imaging Centre, 25 Orde Street, Toronto, Ontario, Canada, M5T 3H7; email: ramy.ayoub@sickkids.ca.

INTRODUCTION

Cranial radiotherapy (CRT) is a vital component of treatment for pediatric brain tumors. For patients with medulloblastoma, combination treatment including CRT leads to almost 90% five-year survival for low- or average-risk patients (*1*). Unfortunately, 90% of survivors treated with CRT also exhibit late effects that affect memory, attention and processing speed (*2, 3*). As a result, these survivors are observed to achieve reduced levels of education, full-time employment and household income (*4*). Options to manage late effects are limited, so research to understand, prevent and treat them is an important priority.

Magnetic resonance imaging (MRI) has demonstrated that cranial irradiation also leads to alterations in brain structure (*5–8*). Deficits in memory capabilities are associated with decreased volume in the hippocampus (*5, 6*), a region critical for learning and memory. In addition, decreased white matter volume after CRT has been shown to predict poor attention and processing speed in pediatric brain tumor survivors (*7–9*). The study of the mechanism of radiation-induced brain structure changes is challenging in clinical populations due to the years over which they may develop, and obvious limitations in experimentally varying CRT prescription. Accordingly, small animal models provide an important alternative for testing hypotheses or candidate interventions. Rodents, in particular, have a faster rate of development than humans and have been shown to recapitulate many of the structural changes in the brain observed in clinical populations treated with CRT (*10*).

Two important observations from cranial irradiation studies in the mouse motivate the current study. First, using MRI to evaluate brain structure after cranial irradiation in juvenile mice, Nieman *et al*. observed that the bulk of radiation-induced volume loss occurs during the early time period after cranial irradiation (~1 week). Subsequently, growth is consistent with sham-irradiated animals, resulting in a persistent deficit into adulthood (*10*). This suggests that the volume losses occurring shortly after cranial irradiation

are predominantly responsible for the long-term volume deficits observed. Interestingly, much of the early volume decrease described by Nieman *et al.* is attributable, at least in part, to the action of p53 (*11*). Knockout of p53 significantly reduces the volume loss observed in the dentate gyrus (DG), olfactory bulbs, pons, optic tract, midbrain, internal capsule and other structures (*11*). It seems likely that this result is linked to the role of p53 in apoptosis after cranial irradiation, which is initiated within hours of treatment.

Second, Beera *et al.* demonstrated that some brain structures, even when nonirradiated, exhibit volume loss after irradiation elsewhere in the brain (*12*). Surprisingly, this was particularly true in white matter. In this case, the anterior commissure exhibited decreased volume after irradiation of the olfactory bulb or subventricular region but not when directly irradiated. This suggests an important contribution of ''off-target'' effects, so that volume loss in a region is not solely a reflection of the radiation dose delivered at that location.

Based on these two observations, we hypothesized that volume loss over the 7–10 days postirradiation would reveal heterogeneity across brain regions. We expected to see two dependencies: 1. regions of white matter may show a pattern of delayed volume loss, owing to the influence of radiation to connected brain regions; and 2. regions known to have a high density of apoptotic cells after irradiation (e.g., the DG) would show early and more extensive volume loss. Previously available imaging data do not capture changes in brain development with sufficient sampling over the days immediately after irradiation to address these hypotheses. The goal of the current work was to map the spatiotemporal volume changes in the mouse brain over the first week after cranial irradiation.

MATERIALS AND METHODS

Mice

Ethics approval was obtained from the animal care committee of the Centre for Phenogenomics (AUP #20-0227H). Wild-type C57BL/6J mice were imaged by MRI at postnatal day (P)14, received 7 Gy (or 0 Gy - sham) at P16, and then were imaged an additional 2–4 times across time points P17 to P28. Mice were grouped into cohorts with different imaging schedules to ensure that, for each time point, imaging data were obtained from at least three different litters but that no mice were imaged more frequently than every two days. This strategy aided in accounting for effects of litter variance (*13*). To place the measured changes in the context of longer-term volume changes, mice (n = 46) were included in which imaging was performed over a more extended period, with time points at P14, P23, P42 and P98.

Cranial Irradiation

In this work, a single 7 Gy (or 0 Gy) dose of cranial irradiation was delivered to a mouse model for pediatric radiotherapy to induce volumetric changes in the brain which recapitulate changes observed in patient populations (*10*). Assuming a fractionation sensitivity α/β of 2 Gy for brain tissue, and that the linear-quadratic model is representative of the radiobiological response (*14*), a single 7 Gy dose corresponds to 16 Gy given in daily doses of 2 Gy (*15*). Although

this dose is slightly lower than typical for treatment of brain tumors, it is in a relevant range for CRT in patients treated for acute lymphoblastic leukemia and we have shown that it leads to volume changes in the mouse brain that are comparable with those observed in brain tumor survivors (*10*). Furthermore, although radiation is typically given via a fractionated dosing scheme in patients, the rapid development rate of the mouse makes this impractical for studies of the effect of cranial irradiation on development (*16*).

At P16, mice were anesthetized with an intraperitoneal (IP) injection of ketamine (100 mg/kg) and xylazine (10 mg/kg) and were placed in a holder comprised of a low-density polyethylene material. To shield the body of the mice from radiation, the polyethylene holder containing the anesthetized mice was placed in a custom-made shield consisting of five layers of lead (153 mm × 110 mm × 7 mm each) stacked both superior and inferior to the holder. We previously calibrated the delivered dose to the head and body within the lead shielding using radiochromic film, where we identified a 15-mm penumbra (*17*). The position of the mice under the lead shield ensured that the penumbra was behind the base of the skull. This positioning exposed the bodies to approximately 10% of the target dose (*17*). Anterior-posterior-posterior-anterior (AP-PA) orientation was achieved through the use of two ^{137}Cs sources (Gammacell® 40 Extractor; Best® Theratronics Ltd., Ottawa, Canada). With the lead shield in place, mice then received a single 7 Gy dose (or 0 Gy) to the whole brain using a ^{137}Cs source at a rate of 0.6 Gy/min (*10, 17, 18*). The Fricke dosimetry system was used to calibrate the ^{137}Cs source (*19*). Calibrations and performance checks on the spectrophotometer and densitometer were carried out using the National Institute of Standards and Technology (NIST)-traceable standard reference materials (*20*).

Magnetic Resonance Image Acquisition and Processing

A cohort of 85 irradiated (male = 30, female = 55) and 38 controls (male = 18, female = 22) were used to assess volume change over the 12 days postirradiation. Data from an additional 24 irradiated (male = 11, female = 13) and 21 controls (male = 12, female = 9) were used to provide longer-term volume data. Data from an additional 24 irradiated and 22 control animals were used to provide longer-term volume data. All MR images were acquired on a multi-channel 7 Tesla (T) MRI scanner equipped with 4 cryocoils that enable simultaneous imaging of 4 mice *in vivo* (*21*). At 24 h prior to the scan, mice received an IP injection of 0.4 mmol/kg of 30 mM manganese chloride (MnCl$_2$) solution to enhance neuroanatomical contrast (*22*). During the scan, mice were placed on a custom-made bed that was maintained at a temperature of 29°C. Mice were anesthetized with a steady source of 1–2% isoflurane.

Images were acquired with the following parameters: T1-weighted, 3D gradient echo sequence, TR = 26 ms, TE = 8.25 ms, flip angle = 26°, field-of-view = 25 × 22 × 22 mm, matrix size = 334 × 294 × 294 [omitting corners of k-space in the phase-encode directions for more rapid acquisition (*23*)], number of averages = 2, total acquisition time = 58 mins, isotropic resolution = 75 μm. At the completion of the scan, mice were moved into a heated cage to allow time to recover from the anesthesia, at which time they were returned to their home cages.

Statistical Analysis

Once the images were acquired, a registration-based image analysis pipeline developed at the Mouse Imaging Centre (MICe, Toronto, Canada) was used to align the images together for quantitative comparison of structure between images. A pre-segmented atlas (*24–27*) was registered to the aligned images to generate structure-wise volumetric data for each individual image across 182 segmented brain regions (combining left and right regions into one, as appropriate) (*28*).

The derived neuroanatomical volumes were fit with a linear mixed-effects model including mouse-, and litter-specific random intercepts and fixed effects accounting for sex, age and treatment (7 Gy vs. 0 Gy)

in the study time course. In our model, a natural spline [degrees of freedom (df) = 2] was used to model the growth of healthy controls over the study time course. In contrast, radiation-induced deviations from normal growth were accounted for by: 1. an offset accounting for possible changes present at day 17; 2. an exponential term modeling volume loss through the early postirradiation period; and 3. a linear change in growth rate to account for long-term growth changes. The total radiation-induced volume change was represented by the following equation:

$$V_{CRT}(t) = V_0(1 - \exp\{-t/\lambda\}) + \beta_{Age}t + \beta_{P17}, \qquad (1)$$

where $V_{CRT}(t)$ represents the volume change for a structure at time t, V_0 represents the total volume change for a structure (which we expected to be negative for irradiated mice and is expressed as a percentage change after normalization to P17 volumes) over the early postirradiation period (exclusive of any long-term growth changes), t represents time in days (with origin at P17), λ represents an exponential time constant (i.e., the time in days required for 63% of the volume change V_0), $\beta_{Age}t$ represents a linear change in growth to account for long-term growth changes, and β_{P17} represents volume change induced already by P17. An estimate for the λ coefficient was obtained by a search over the range 1 to 8 days (at 0.2-day intervals) followed by interpolation to minimize sum of square residuals. The interpolated λ coefficient was then used to estimate the V_0 term for a given structure.

After fitting the model to all structure volume time courses, the analysis proceeded in two serial steps. In the first step, we identified all structures that exhibited a significant effect of radiation treatment. For this purpose, we employed a likelihood ratio test, comparing the complete linear mixed effects model with an equivalent model that excluded the terms representing radiation-induced change. The Satterthwaite approximation was subsequently used to estimate the degrees of freedom for evaluation of significance for individual coefficients (29). We corrected for multiple comparisons using the false discovery rate (FDR) method (30). In the second step, within the identified structures, we evaluated possible differences in time constant (λ) or magnitude of early volume change (V_0). We will refer to the V_0 term as the volume change induced by cranial irradiation, and the $\beta_{Age}t$ term as changes in growth rate.

Dependence of volume change or timing on of the volume change time course was assessed in two ways: 1. brain structures were separated into four groups comprised of gray matter, white matter, cerebral spinal fluid (CSF), and uncategorized atlas structures to compare differences in the timing and magnitude between them; 2. brain structures were separated based on results from de Guzman *et al.* (11), which indicated that p53-knockout led to a reduction in the extent of radiation-induced volume loss in certain brain regions. For the latter, brain structures were separated into two groups based on sensitivity or insensitivity of the radiation-induced change to p53 loss. The two groups were established using the previously published results from de Guzman *et al.* (11) by choosing brain structures with a t-statistic in the top versus the bottom third of the distribution, respectively, labeled sensitive and insensitive to p53-knockout. Results did not exhibit a normal distribution across the V_0 and λ terms, so we evaluated potential group difference through a non-parametric Mann-Whitney U test (31).

RESULTS

Widespread Volume Losses Present in Adulthood after Cranial Irradiation at a Juvenile Age

Using longitudinal MRI, we identified 101 structures exhibiting a significant difference in the volume change time course due to cranial irradiation (using a threshold of q < 0.01 based on a likelihood ratio test). This included 62% of gray matter structures in the atlas (82 of 134 regions), 28% of white matter structures (11 of 39 regions), 100% of CSF structures (4 of 4 regions) and 67% of the uncategorized atlas structures (4 of 6 regions).

At P98, long-term volume changes showed widespread deficits in irradiated mice when compared to controls (Fig. 1). Notable volume changes included the olfactory bulb (granule cell layer) (14.9%), pituitary gland (12.5%), corpus callosum (11.1%) and DG (molecular layer) (10.1%). Comparative analyses of differences in radiation-induced volume loss or time constants were subsequently conducted using only these 101 identified structures. A summary of the results for all structures is provided in Supplementary Table S1 (https://doi.org/10.1667/RADE-21-00013.1.S1).

Crainal Irradiation Leads to a Delayed Onset of Volume Loss which Manifests over the First Week Postirradiation

To better understand the evolution of radiation-induced volume changes, we calculated the rate of change of structure volume for each structure over time (in mm³/day or %/day as computed from the linear mixed-effects model), thus highlighting times of greatest difference in growth relative to controls. As shown in Fig. 2, few changes in volume were observed at P17 (one day after irradiation). Subsequently, volume loss, as characterized by the exponential term, was observed over much of the brain. Widespread growth differences waned over the course of a few days so that, by P22, few differences were observed throughout the remainder of the early time period after irradiation. Overall, these results indicate that there is an initial 1- to 2-day delay after irradiation in which volume is not significantly perturbed, after which volume change proceeds over the course of ~4 days. After this time, growth is largely normal in irradiated mice. This demonstrates the expected result that the long-term deficits in volume after CRT are largely a result of the volume losses which manifest over the early time period postirradiation, rather than a persistently decreased growth (10).

White and Gray Matter Differences in the Timing of Volume Loss in the Week Postirradiation

The magnitude of cumulative volume loss through the days immediately after irradiation (as assessed by the V_0 coefficient) ranged from 4 to 27% of P17 volume. We observed a trend in the magnitude of volume loss, where the median volume loss for gray matter structures was 9.7%, while white matter structures exhibited a median of 12.1% volume loss after CRT ($P = 0.056$, not significant) (Fig. 3). Across the brain, the median magnitude of volume loss was approximately 10%. Among the largest decreases were those observed in ventricular regions, including the lateral ventricles (27% volume decrease) and the third ventricle (26% volume decrease). Figure 4A and B represents structures exhibiting ''small'' and ''large'' volume changes over the postirradiation time period, respectively.
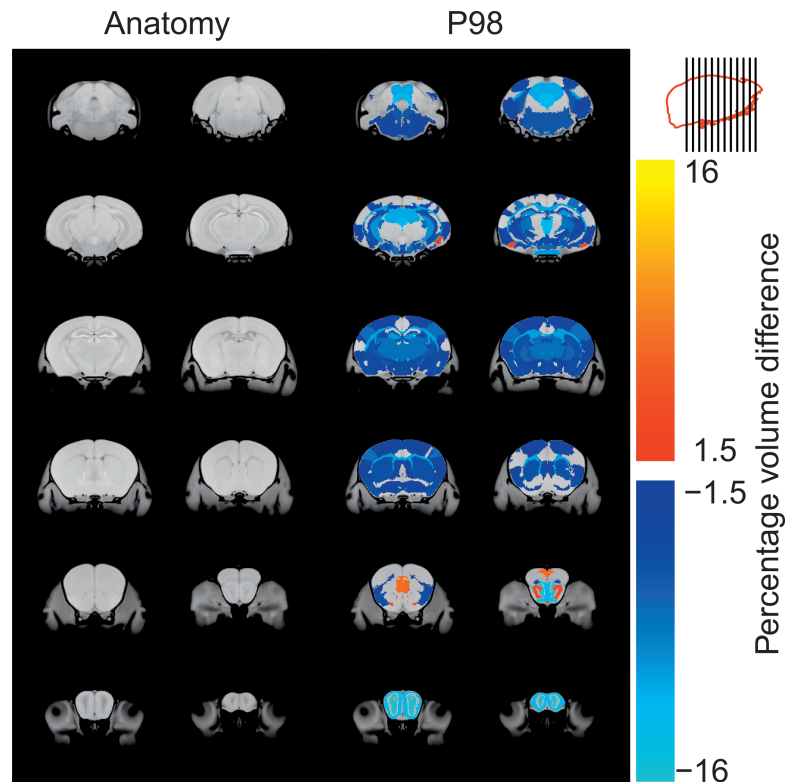
FIG. 1. Percentage volume differences across irradiated and control mice at the P98 time point after cranial irradiation at a juvenile age. Images under the ''Anatomy'' header represent coronal slices of a consensus average brain image. The image panels from left to right and top to bottom represent consecutive coronal slices, proceeding from caudal to rostral slices. The position of the slices can be seen in the sagittal brain legend (top right). Images under the ''P98'' header represent the same set of slices, with a color scale superimposed to represent radiation-induced volume changes. The color scale shows percentage volume difference by structure across irradiated and control mice. Results demonstrate widespread volume losses.

A significant difference in the timing of volume loss across gray and white matter structures was observed ($P = 0.023$), where the median time constant value was 2.7 and 3.8 days, respectively (Fig. 5). Figure 4C and D represent structures exhibiting ''fast'' and ''slow'' emerging volume changes over the postirradiation period.

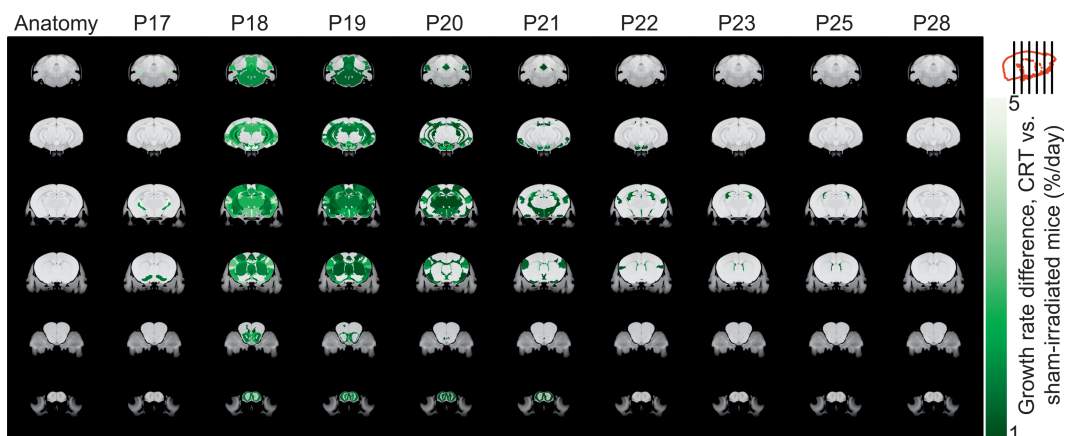In addition to the grouping of gray and white matter, we also compared the timing and magnitude of volume loss

FIG. 2. Structure-wise analysis of growth differences in irradiated mice during the early time period after cranial irradiation. Using our linear mixed-effects model, we calculated the percentage change in growth rate attributable to cranial irradiation. All values (in mm^3/day) were normalized with respect to P17 volume estimates. The position of the slices can be seen in the sagittal brain legend in the upper right. Results demonstrated $\sim$2 days in the onset of volume loss after cranial irradiation, which then manifests over the course of $\sim$4 days. Early volume losses were largely followed by normal growth.
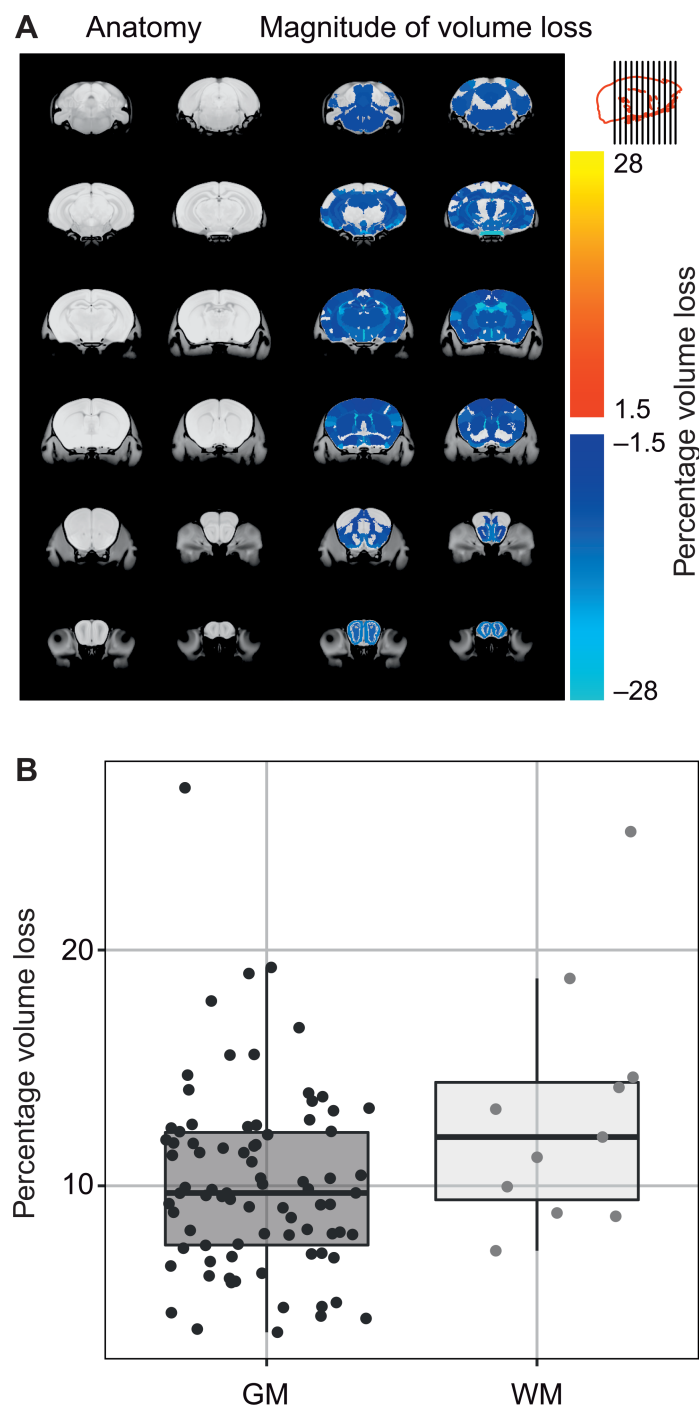
FIG. 3. Examination of differences in the magnitude of volume loss across brain structures demonstrating a significant difference in the volume change time course due to cranial irradiation (using a threshold of q < 0.01 based on a likelihood ratio test). Panel A: Structure-wise analysis of the magnitude of volume loss through the early postirradiation period. To examine the magnitude of initial volume loss, the normalized V_0 term was visualized, indicating the relative extent of loss that occurred for each structure. Results indicated a trend in the magnitude of volume loss across gray and white matter structures ($P = 0.056$, not significant), where the median volume loss postirradiation was 9.7% and 12.1%, respectively. Panel B: Plot recapitulates results from panel A, but specifically compares gray and white matter differences in the magnitude of volume loss. The x-axis represents brain regions placed into two groups based on classification as gray matter (darker points) or white matter (lighter points). The y-axis represents the percentage volume loss. Points in the plot represent distinct brain regions.
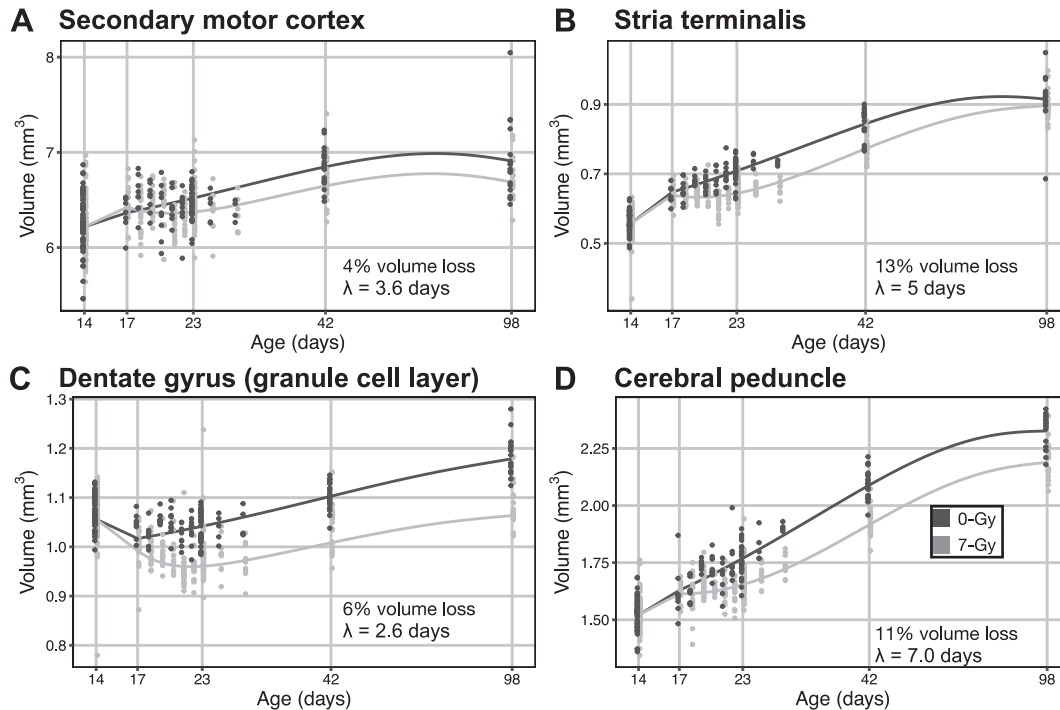
FIG. 4. Visualization of volume change over time in representative brain regions. Adjusted volumes were generated by subtracting the mouse-, and litter-specific random intercepts from raw data and then visualized by group with fit lines. For each plot (panels A–D), the x-axis represents age, while y-axis represents the volume of voxels within the structures. Points within the plots represent individual mice, with darker points representing sham controls, and lighter points representing mice receiving cranial irradiation. Points were fit using the linear mixed effects model, where a natural spline was used to model the time course of normal growth. Panels A and B: Plots represent structures exhibiting "small" and "large" magnitude volume changes over the time period postirradiation, respectively. The secondary motor cortex exhibited a small volume loss of ~4% after cranial irradiation, while the stria terminalis exhibited a large volume loss of ~13%. Panels C and D: Plots represent structures exhibiting "fast" and "slow" emerging volume changes over the time period postirradiation, respectively. The dentate gyrus (granule cell layer) exhibited fast emerging volume changes with a λ value of 2.6 days, while the cerebral peduncle had a more protracted emergence of volume change, with a λ value of 7.0 days.

across regions previously shown to have altered radiation-induced volume changes after knockout of p53. This demonstrated no significant differences in either the timing ($P = 0.180$) or magnitude ($P = 0.235$) of volume loss (Fig. 6).

DISCUSSION

Radiation therapy is vital in the treatment of brain cancer, but is associated with late effects, i.e., delayed side effects that appear months or years after the onset of treatment, which are associated with decreased quality of life (2, 3, 9, 32, 33). These late effects are particularly prevalent in pediatric brain tumor patients (34), and have been shown to include progressive cognitive deficits (7). Most notably, deficits in memory, attention and processing speeds have been observed in pediatric patients treated for brain tumors (35). These cognitive deficits have been recapitulated in mouse models for pediatric radiotherapy. For example, juvenile-irradiated mice have exhibited decreased performance in spatial and working memory in adulthood (35, 36), as well as long-term changes in the structure of associated brain regions (37, 38).

To better understand the emergence of structural differences observed in the brain after irradiation, this study spatiotemporally characterized volume losses over the early postirradiation period across the brain. We determined that timing of radiation-induced volume loss appeared to differ across gray and white matter, with white matter volume loss emerging approximately 40% slower than gray matter volume loss. We also found a trend indicating larger volume loss in white matter compared to gray matter, as expected from previously published findings (10, 18). On the other hand, an examination of potential differences in these parameters between regions previously identified as sensitive to p53-mediated CRT-induced volume loss demonstrated no significant differences. Together, these results suggest that apoptosis alone does not explain the widespread volume losses observed after irradiation. It seems likely that other radio-responses, e.g., secondary to increased inflammation (39) and decreased neurogenesis (40), play an important role in contributing to the volume loss and time course observed.

Unexpectedly, volume decreases in the CSF of the ventricles were found to be particularly large over the week
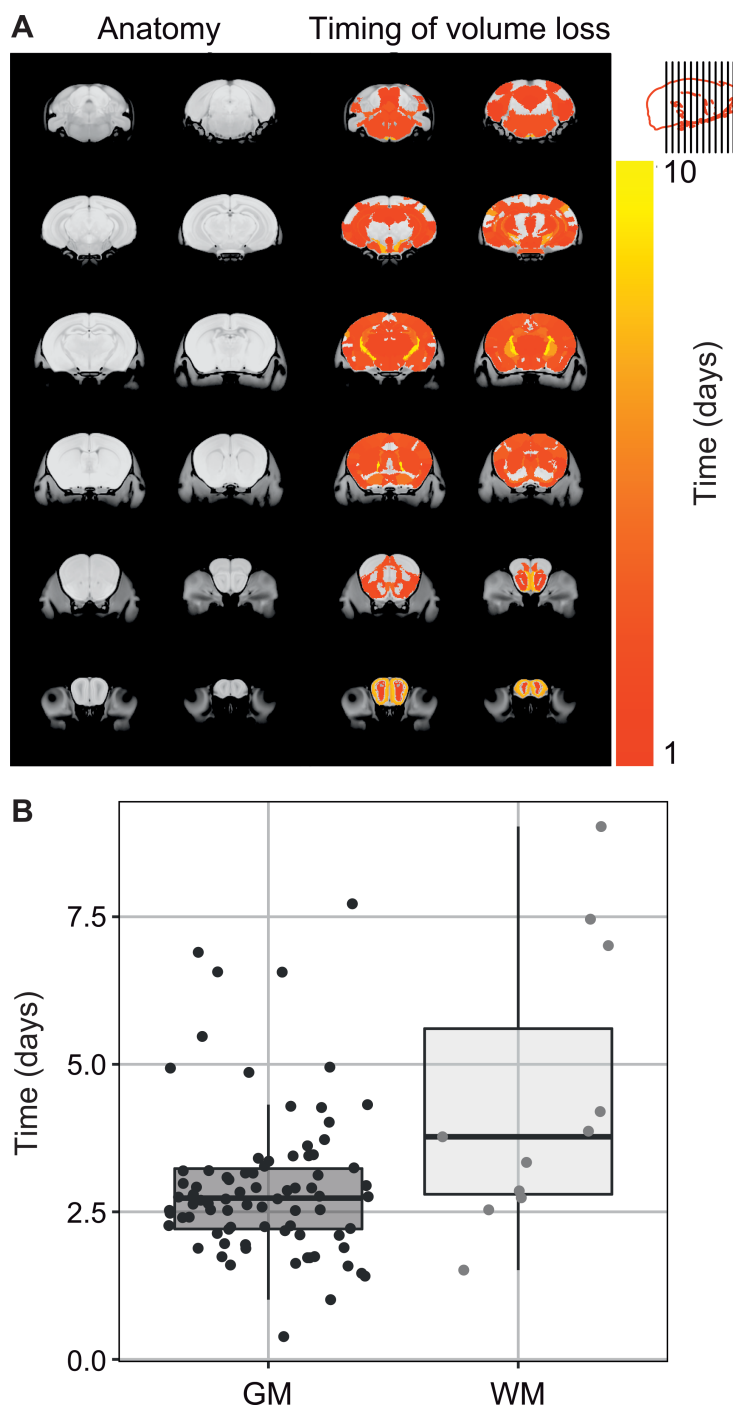
FIG. 5. Examination of differences in the timing of volume loss across brain structures demonstrating a significant difference in the volume change time course due to CRT (using a threshold of q < 0.01 based on a likelihood ratio test). Panel A: Structure-wise analysis of the timing of volume loss after cranial irradiation. The λ value unique to each structure is shown in the color map, and indicates the days required for 63% of the volume loss V_0 to occur. Results indicated a significant difference in the timing of volume loss across gray and white matter structures ($P = 0.023$), with white matter volume loss emerging slower than gray matter volume loss. Panel B: Plot recapitulates results from panel A, but specifically compares gray and white matter differences in the timing of volume loss. The x-axis represents brain regions placed into two groups based on classification as gray matter (darker points) or white matter (lighter points). The y-axis represents the percent volume loss. Points in the plot represent distinct brain regions.
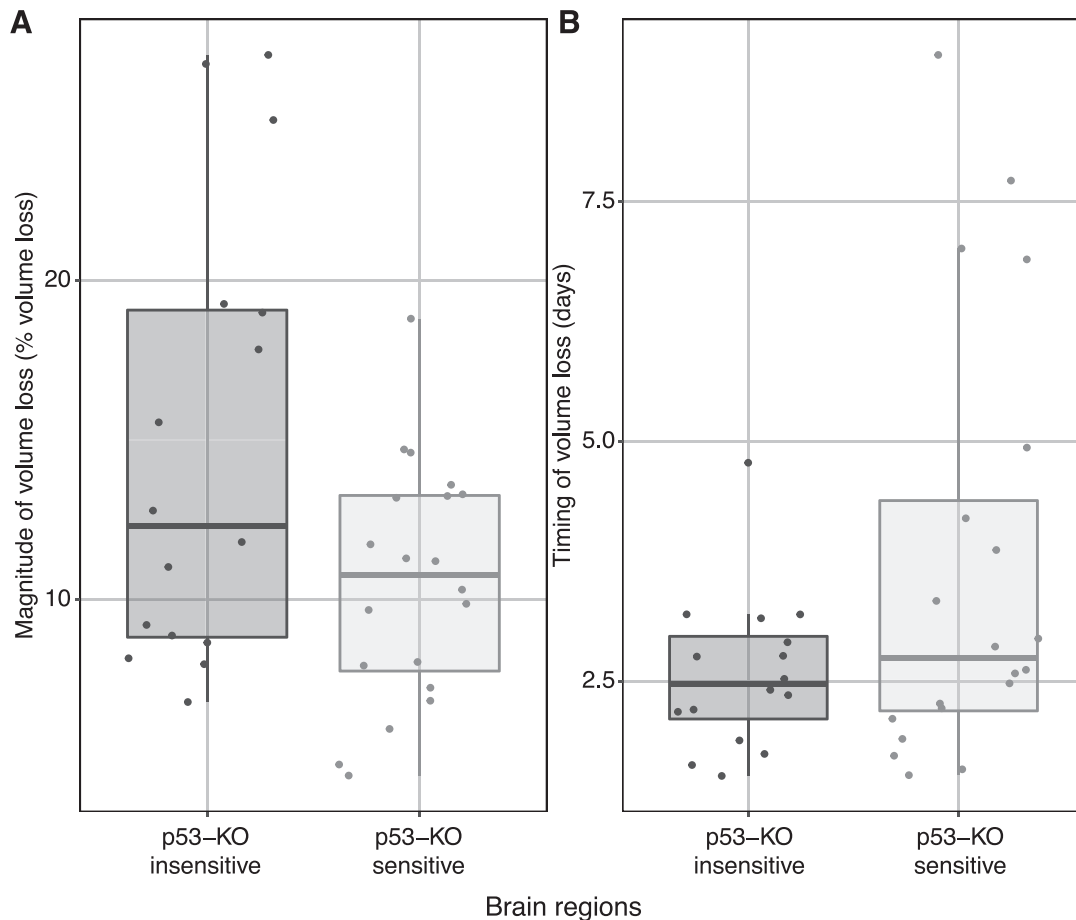
FIG. 6. Examination of differences in the timing and magnitude of volume loss across regions based on influence of p53-knockout on radioresponse. Panel A: The x-axis represents brain regions placed into two groups based on elevated (lighter points) or limited sensitivity (darker points) to p53-knockout. The y-axis represents the percentage volume loss. Points in the plot represent distinct brain regions. Results indicated no significant differences in the magnitude of volume loss across brain regions. Panel B: The same plot as panel A but with the y-axis derived from the timing of volume loss in days. Points in the plot represent the brain regions which exhibited a significant corrected effect of cranial irradiation during the early postirradiation period. Results indicated no significant differences in the timing of volume loss based on this grouping of structures.

after irradiation. Typically, in the presence of brain tissue atrophy, CSF spaces are enlarged in relationship to the intracranial volume to compensate for tissue volume loss (*41*). Instead, we demonstrate a large decrease in the volume of CSF structures. This result may stem from the fact that this study is examining changes in brain structure in a developmental context, whereas atrophy is more frequently observed in the context of neurodegeneration associated with normal aging or adult-onset pathologies. A possible mechanism for this result might stem from radiation-induced damage to the choroid plexus (CP). This structure lies within the lateral and fourth ventricles in the brain and is known to generate and clean the CSF (*42*). Damage to the CP may lead to decreases in the production of CSF, leading to the observed decreases in ventricular volumes, with possible consequences for the brain. Unfortunately, it is not possible to assess the CP through the image registration and analysis steps used in this study since the CP is highly variable in morphology from one mouse to the next.

The characterization of the timing of volume loss throughout the time period postirradiation demonstrated a delay before volume loss was observed (i.e., change was not present at P17, but began emerging thereafter). This is of interest, since it has previously been shown that cellular apoptosis is extensive within 8 h of irradiation in the DG and the subventricular zone (SVZ) (*11*). It is possible that the temporal delay observed is consistent with the duration of apoptotic processes (*43*) and subsequent clearance of cellular debris, which is more protracted. Thus, although the initial phase of apoptosis is observed within hours, any resulting volume loss to which structural MRI is sensitive is expected to occur over a more extended period. Nonetheless, while the timing of volume loss is not inconsistent with apoptosis, much of the brain, including regions with more limited apoptosis, exhibited a similar pattern of volume loss, suggesting other contributing factors.

Several different mechanisms and their combination may contribute to the volume losses observed, with potential for significant regional dependencies. For example, CRT in

pediatric populations is also associated with elevated risk for endocrine late effects, often associated with growth failure, obesity or altered pubertal timing (*44, 45*). In our mice, an examination of the long-term effects of cranial irradiation on the pituitary gland demonstrated a 12.5% volume loss. Hypopituitarism would have widespread implications for brain development (*46, 47*). Radiation-induced growth hormone deficiency is associated with decreased IQ scores and lower socioeconomic status (*47, 48*). Radiation-induced changes in both the population and activation state of microglial cells is reported to be time-dependent and might also be expected to produce widespread volume changes (*49, 50*). More locally, decreased neurogenesis after radiotherapy and its possible association with cognitive performance has been widely studied in animal models. Even at low doses, cranial irradiation disrupts the neurogenic niche within the DG of the hippocampus (*51, 52*). The radiation-induced damage to this niche is associated with increased apoptosis (*53, 54*), decreased cell proliferation (*54, 55*) and decreased neuronal differentiation (*56*). Volume changes within the hippocampus therefore, at least in part, are likely reflective of apoptotic and neurogenic changes (*11*). Lastly, we note that alterations in dendritic pruning and synaptic density have been reported postirradiation, which could contribute volume change in regions with high dendrite and synapse density (*37, 38, 57*).

The differences across gray and white matter in the timing of volume loss from this study complement results discussed by Beera *et al.* (*12*). In that work, spatial localization of radiation was used to demonstrate that a significant portion of volume loss in white matter regions may stem from off-target effects (i.e., secondary to radiation delivered in other brain regions) (*12*). The finding that gray matter regions exhibit volume losses at an earlier time than do white matter regions is consistent with the hypothesis that white matter volume loss may be partly dependent on damage in connected gray matter. For instance, it is possible that radiation-induced damage or apoptosis of neuronal cell bodies leads to degeneration of, or to downstream structural changes in, associated axons.

The data obtained in this study provides a more complete description of the time course of brain structure change after cranial irradiation in a mouse model than was previously available. We have shown that a delay in the onset of volume loss is present after cranial irradiation, with volume losses manifesting over the course of a week with an average exponential time constant of 4 days. Furthermore, we observed differences in the timing of volume between gray and white matter, with slightly delayed volume losses seen in white matter regions.

SUPPLEMENTARY INFORMATION

Table S1. Summary of model output for all structures.

REFERENCES

1. Thomas A, Noel G. Medulloblastoma: optimizing care with a multidisciplinary approach. J Multidiscip Healthc 2019; 12:335–47.

2. Robinson KE, Fraley CE, Pearson MM, Kuttesch JF, Compas BE. Neurocognitive late effects of pediatric brain tumors of the posterior fossa: A quantitative review. J Int Neuropsychol Soc 2012; 19:44–53.

3. Palmer SL, Hassall T, Evankovich K, Mabbott DJ, Bonner M, Deluca C, et al. Neurocognitive outcome 12 months following cerebellar mutism syndrome in pediatric patients with medulloblastoma. Neuro Oncol 2010; 12:1311–7.

4. Chevignard M. Quality of survival after childhood medulloblastoma. Ann Phys Rehabil Med 2014; 57.

5. Jayakar R, King TZ, Morris R, Na S. Hippocampal volume and auditory attention on a verbal memory task with adult survivors of pediatric brain tumor. Neuropsychology 2015; 29:303–19.

6. Decker AL, Szulc KU, Bouffet E, Laughlin S, Chakravarty MM, Skocic J, et al. Smaller hippocampal subfield volumes predict verbal associative memory in pediatric brain tumor survivors. Hippocampus 2017; 27:1140–54.

7. Palmer SL. Neurodevelopmental impact on children treated for medulloblastoma: A review and proposed conceptual model. Dev Disabil Res Rev 2008; 14:203–10.

8. Palmer SL, Armstrong C, Onar-Thomas A, Wu S, Wallace D, Bonner MJ, et al. Processing speed, attention, and working memory after treatment for medulloblastoma: An international, prospective, and longitudinal study. J Clin Oncol 2013; 31:3494–500.

9. Reddick WE, White HA, Glass JO, Wheeler GC, Thompson SJ, Gajjar A, et al. Developmental model relating white matter volume to neurocognitive deficits in pediatric brain tumor survivors. Cancer 2003; 97:2512–9.

10. Nieman BJ, de Guzman AE, Gazdzinski L, Lerch JP, Chakravarty MM, Pipitone J, et al. White and gray matter abnormalities after cranial radiation in children and mice. Int J Radiat Oncol Biol Phys 2015; 93:882–91.

11. de Guzman AE, Ahmed M, Li Y, Wong S, Nieman BJ. p53 Loss mitigates early volume deficits in the brains of irradiated young mice. Int J Radiat Oncol Biol Phys 2019; 103:511–20.

12. Beera K, Li Y, Dazai J, Stewart J, Egan S, Ahmed M, et al. Altered brain morphology after focal radiation reveals impact of off-target effects: implications for white matter development and neurogenesis. Neuro Oncol 2017; 20:788–98.

13. Tanaka T. Effects of litter size on behavioral development in mice. Reprod Toxicol 1998; 12:613–7.

14. Brand DH. The linear-quadratic model and implications for fractionation. Clin Oncol (R Coll Radiol) 2019; 31:673–7.

15. Barendsen GW. Dose fractionation, dose rate and iso-effect relationships for normal tissue responses. Int J Radiat Oncol Biol Phys 1982; 8:1981–97.

16. Semple BD, Blomgren K, Gimlin K, Ferriero DM, Noble-Haeusslein LJ. Brain development in rodents and humans: Identifying benchmarks of maturation and vulnerability to injury across species. Prog Neurobiol 2013; 106:1–16.

17. de Guzman AE, Gazdzinski LM, Alsop RJ, Stewart JM, Jaffray DA, Wong CS, et al. Treatment age, dose and sex determine

neuroanatomical outcome in irradiated juvenile Mice. Radiat Res 2015; 183:541.

18. Gazdzinski LM, Cormier K, Lu FG, Lerch JP, Wong CS, Nieman BJ. Radiation-induced alterations in mouse brain development characterized by magnetic resonance imaging. Int J Radiat Oncol Biol Phys 2012; 84:e631–8.

19. Olszanski A, Klassen NV, Ross CK, Shortt KR. The IRS Fricke dosimetry system. PIRS-0815. Ottawa, Ontario, Canada: Institute for National Measurement Standards, National Research Council; 2002.

20. Travis JC, Smith MV, Rasberry SD, Kramer GW. Technical specifications for certification of spectrophotometric NTRMs. NIST Special Publication 2000; 260:140.

21. Bock N, Nieman BJ, Bishop J, Henkelman RM. In vivo multiple-mouse MRI at 7 Tesla. Magn Reson Med 2005; 54:1311–6.

22. Koretsky AP, Silva AC. Manganese-enhanced magnetic resonance imaging (MEMRI). NMR Biomed 2004; 17:527–31.

23. Spencer Noakes TL, Henkelman RM, Nieman BJ. Partitioning k-space for cylindrical three-dimensional rapid acquisition with relaxation enhancement imaging in the mouse brain. NMR Biomed 2017; 30:e3802.

24. Dorr AA, Lerch JP, Spring S, Kabani N, Henkelman RM. High resolution three-dimensional brain atlas using an average magnetic resonance image of 40 adult C57Bl/6J mice. Neuroimage 2008; 42:60–9.

25. Richards K, Watson C, Buckley RF, Kurniawan ND, Yang Z, Keller MD, et al. Segmentation of the mouse hippocampal formation in magnetic resonance images. Neuroimage 2011; 58:732–40.

26. Ullmann JF, Watson C, Janke AL, Kurniawan ND, Reutens DC. A segmentation protocol and MRI atlas of the C57BL/6J mouse neocortex. Neuroimage 2013; 78:196–203.

27. Steadman PE, Ellegood J, Szulc KU, Turnbull DH, Joyner AL, Henkelman RM, et al. Genetic effects on cerebellar structure across mouse models of autism using a magnetic resonance imaging atlas. Autism Res 2013; 7:124–37.

28. Chakravarty MM, Steadman PE, Eede MCV, Calcott RD, Gu V, Shaw P, et al. Performing label-fusion-based segmentation using multiple automatically generated templates. Human Brain Mapp 2012; 34:2635–54.

29. Satterthwaite FE. An approximate distribution of estimates of variance components. Biometrics 1946; 2:110–4.

30. Genovese CR, Lazar NA, Nichols T. Thresholding of statistical maps in functional neuroimaging using the false discovery rate. Neuroimage 2002; 15:870–8.

31. R: A language and environment for statistical computing. Vienna, Austria: R Core Team; 2013. (http://www.R-project.org/)

32. Mitby PA, Robison LL, Whitton JA, Zevon MA, Gibbs IC, Tersak JM, et al. Utilization of special education services and educational attainment among long-term survivors of childhood cancer. Cancer 2003; 97:1115–26.

33. Nathan PC. Guidelines for identification of, advocacy for, and intervention in neurocognitive problems in survivors of childhood cancer. Arch Pediatr Adolesc Med 2007; 161:798.

34. Askins MA, Bartlett III MD. Preventing neurocognitive late effects in childhood cancer survivors. J Child Neurol 2008; 23:1160–71.

35. Ayoub R, Ruddy RM, Cox E, Oyefiade A, Derkach D, Laughlin S, et al. Assessment of cognitive and neural recovery in survivors of pediatric brain tumors in a pilot clinical trial using metformin. Nat Med 2020; 26:1285–94.

36. Alexander TC, Butcher H, Krager K, Kiffer F, Groves T, Wang J, et al. Behavioral effects of focal irradiation in a juvenile murine model. Radiat Res 2018; 189:605–17.

37. Ruddy RM, Derkach D, Dadwal P, Morshead CM. Cranial irradiation in juvenile mice leads to early and sustained defects in

the stem and progenitor cell pools and late cognitive impairments. Brain Res 2020; 1727:146548.

38. Mizumatsu S, Monje ML, Morhardt DR, Rola R, Palmer TD, Fike JR. Extreme sensitivity of adult neurogenesis to low doses of X-irradiation. Cancer Res 2003; 63:4021–7.

39. Lumniczky K, Szatm'ari T, S'afr'any G. Ionizing radiation-induced immune and inflammatory reactions in the brain. Front Immunol 2017; 8:517.

40. Monje ML, Vogel H, Masek M, Ligon KL, Fisher PG, Palmer TD. Impaired human hippocampal neurogenesis after treatment for central nervous system malignancies. Ann Neurol 2007; 62:515–20.

41. de Vis JB, Zwanenburg JJ, van der Kleij LA, Spijkerman JM, Biessels GJ, Hendrikse J, et al. Cerebrospinal fluid volumetric MRI mapping as a simple measurement for evaluating brain atrophy. Eur Radiol 2015; 26:1254–62.

42. Hofman FM, Chen TC. Choroid plexus: Structure and function. The choroid plexus and cerebrospinal fluid. Cambridge, MA: Academic Press; 2016. p. 29–40.

43. Lockshin RA, Zakeri Z. Cell death (apoptosis, programmed cell death). Directions in Science 2002; 1:41–4.

44. Aslan IR, Cheung CC. Early and late endocrine effects in pediatric central nervous system diseases. J Pediatr Rehabil Med 2014; 7:281–94.

45. Bieri S, Sklar C, Constine L, Bernier J. Late effects of radiotherapy on the neuroendocrine system. (Article in French). Cancer Radiother 1997; 1:706–16.

46. Agha A, Sherlock M, Brennan S, O'Connor SA, O'Sullivan E, Rogers B, et al. Hypothalamic-pituitary dysfunction after irradiation of nonpituitary brain tumors in adults. J Clin Endocrinol Metab 2005; 90:6355–60.

47. Darzy KH. Radiation-induced hypopituitarism. Curr Opin Endocrinol Diabetes Obes 2013; 20:342–53.

48. Meyer-Bahlburg HFL, Feinman JA, MacGillivray MH, Aceto T. Growth hormone deficiency, brain development, and intelligence. Am J Dis Child 1978; 132:565–72.

49. Moravan MJ, Olschowka JA, Williams JP, O'Banion MK. Cranial irradiation leads to acute and persistent neuroinflammation with delayed increases in T-cell infiltration and CD11c expression in C57BL/6 mouse brain. Radiat Res 2011; 176:459–73.

50. Schindler MK, Forbes ME, Robbins ME, Riddle DR. Aging-dependent changes in the radiation response of the adult rat brain. Int J Radiat Oncol Biol Phys 2008; 70:826–34.

51. Monje M. Cranial radiation therapy and damage to hippocampal neurogenesis. Dev Disabil Res Rev 2008; 14:238–42.

52. Chen SCJ, Abe Y, Fang PT, Hsieh YJ, Yang YI, Lu TY, et al. Prognosis of hippocampal function after sub-lethal irradiation brain injury in patients with nasopharyngeal carcinoma. Sci Rep 2017; 7:14697.

53. Li Q, Cheng Z, Wong S. Differential apoptosis radiosensitivity of neural progenitors in adult mouse hippocampus. Int J Mol Sci 2016; 17:970.

54. Sun AM, Li CG, Han YQ, Liu QL, Xia Q, Yuan YW. X-ray irradiation promotes apoptosis of hippocampal neurons through up-regulation of Cdk5 and p25. Cancer Cell Int 2013; 13:47.

55. Mineyeva OA, Bezriadnov DV, Kedrov AV, Lazutkin AA, Anokhin KV, Enikolopov GN. Radiation induces distinct changes in defined subpopulations of neural stem and progenitor cells in the adult hippocampus. Front Neurosci 2019; 12:1013.

56. Konirova J, Cupal L, Jarosova S, Michaelidesova A, Vachelova J, Davidkova M, et al. Differentiation induction as a response to irradiation in neural stem cells in vitro. Cancers 2019; 11:913.

57. Gibson EM, Monje M. Microglia in cancer therapy-related cognitive impairment. Trends Neurosci 2021; 44:441–51.